Elsevier Editorial System(tm) for Earth and Planetary Science Letters
Manuscript Draft

Manuscript Number: EPSL-D-08-01057R1

Title: Trench-parallel fast axes of seismic anisotropy due to fluid-filled cracks in subducting slabs

Article Type: Regular Article

Keywords: Shear wave splitting; High pressure metamorphism; Vein; Serpentinite; Eclogite; Dehydration

Corresponding Author: Dr David Healy, PhD

Corresponding Author's Institution: Curtin University of Technology

First Author: David Healy, PhD

Order of Authors: David Healy, PhD; Steven M Reddy; Nicholas E Timms; Erin M Gray; Alberto Vitale Brovarone

Abstract: Subducting slabs experience deformation and metamorphism as they descend into the upper mantle. The presence of hydrous minerals gained through the interaction with sea water at mid-ocean ridges, transform faults or the outer rise ensures that dehydration reactions will be important at deeper levels. We describe field evidence for brittle hydrofracture in previously subducted rocks from the Western Alps, with a free aqueous fluid phase produced by dehydration reactions in the host blueschists and serpentinites. The protracted history of dehydration reactions, ductile deformation, fluid flow and brittle vein formation in these rocks implies that fluid-filled cracks are continuously produced within the dehydration window. The presence of abundant fluid-filled cracks at these depths has important implications for the seismic anisotropy generated within slabs, which has largely been overlooked. The effects of fluid-filled crack damage on the elastic properties of a blueschist and serpentinite within the slab at depth have been modelled, and show a significant rotation of the fast axes of P and S1 waves to be trench-parallel for receiving stations in the forearc,

above the dehydrating portion of the slab. This model provides an alternative explanation for supra-subduction zone seismic anisotropy that does not require high-stress, high-water conditions, or trench-parallel flow in the supra-subduction zone mantle wedge.

Trench-parallel fast axes of seismic anisotropy due to fluid-filled cracks in subducting slabs

David Healy[1*], Steven M. Reddy[1], Nicholas E. Timms[1], Erin M. Gray[1] and Alberto Vitale Brovarone[2]

[1]The Institute for Geoscience Research, Department of Applied Geology, Curtin University of Technology, GPO Box U1987, Perth WA 6845, Australia

[2]Università degli Studi di Torino, Dip. di Scienze Mineralogiche e Petrologiche, Via Valperga Caluso, 35, 10125 Torino, Italy

[*]Corresponding author e-mail: d.healy@curtin.edu.au

Tel: +61 (0)8 9266 7969

Fax: +61 (0)8 9266 3153

Abstract

Subducting slabs experience deformation and metamorphism as they descend into the upper mantle. The presence of hydrous minerals gained through the interaction with sea water at mid-ocean ridges, transform faults or the outer rise ensures that dehydration reactions will be important at deeper levels. We describe field evidence for brittle hydrofracture in previously subducted rocks from the Western Alps, with a free aqueous fluid phase produced by

dehydration reactions in the host blueschists and serpentinites. The protracted history of dehydration reactions, ductile deformation, fluid flow and brittle vein formation in these rocks implies that fluid-filled cracks are continuously produced within the dehydration window. The presence of abundant fluid-filled cracks at these depths has important implications for the seismic anisotropy generated within slabs, which has largely been overlooked. The effects of fluid-filled crack damage on the elastic properties of a blueschist and serpentinite within the slab at depth have been modelled, and show a significant rotation of the fast axes of P and S_1 waves to be trench-parallel for receiving stations in the forearc, above the dehydrating portion of the slab. This model provides an alternative explanation for supra-subduction zone seismic anisotropy that does not require high-stress, high-water conditions, or trench-parallel flow in the supra-subduction zone mantle wedge.

Keywords

Shear wave splitting; High pressure metamorphism; Vein; Serpentinite; Dehydration; Eclogite

1. Introduction

It is widely accepted that subducting lithospheric plates undergo metamorphism and deformation as they descend into the mantle. Theoretical arguments (e.g. Peacock, 1993; Hacker et al., 2003a, 2003b) and laboratory experiments (e.g. Schmidt & Poli, 1998), combined with seismological observations from current subduction zones (e.g. Abers et al., 2006) and geological observations from exhumed but previously subducted rocks (e.g. Scambelluri et al., 1995), confirm that slabs undergo profound changes in mineralogy,

45 structure, rheology and fluid-content during their downward journey. The full implications of
46 these changes have yet to be fully understood.

47 Dislocation-controlled deformation of olivine, the most abundant mineral in the
48 Earth's upper mantle, leads to strain-induced lattice preferred orientation (LPO) and
49 anisotropy in the elastic properties of the bulk rock (Birch, 1960). Observations of anisotropy
50 in the velocities of seismic waves can be used to infer the kinematics and dynamics of flow in
51 the mantle (Savage, 1999; Park & Levin, 2002). Above subduction zones, seismic anisotropy
52 commonly varies across the arc, with backarc and forearc regions displaying trench-
53 perpendicular and trench-parallel fast axes, respectively (Nakajima & Hasegawa, 2004; Long
54 & van der Hilst, 2006). This variation in polarization directions has been interpreted as
55 differences in the alignment of olivine [100] *a*-axes.

56 The origin of trench-parallel fast directions is controversial and may reflect flow of the
57 mantle parallel to the trench, associated with slab rollback (Schellart, 2004; Long & Silver,
58 2008) or by three-dimensional (3D) flow caused by slab topography (Kneller & van Keken,
59 2007) or locally driven thermal convection (Lowman et al., 2007). Field and microstructural
60 evidence from mantle rocks exposed along the exhumed Talkeetna arc in Alaska show that
61 trench-parallel fast directions are due to slip on (001)[100] (Mehl et al., 2003). However,
62 experimental studies of olivine deformation (Jung & Karato, 2001) indicate that high water
63 content and high stress, which may be present in the supra-subduction mantle wedge, lead to
64 Type B olivine fabrics with (010) [001] slip. Type B olivine fabrics produce trench-parallel
65 alignment of the seismically fast [100] direction, at 90° to the kinematic flow direction
66 associated with trench-normal corner flow in the mantle wedge above the down-going slab
67 (Kneller et al., 2005).

68 In most models used to explain supra-subduction seismic anisotropy, the contribution
69 of the subducting slab has been neglected. A recent exception is the model by Faccenda et al.

(2008), who suggested that hydration of sub-vertical fault zones in the upper slab could produce seismic anisotropy due largely to the presence of talc, which has been shown to be highly anisotropic in its elastic properties (Mainprice et al., 2008). Another recent model proposes a relatively thin (10-20 km) zone of dislocation creep above the slab in a mantle wedge dominated by diffusion creep (Katayama, 2009). In this paper, we combine new field data and theoretical calculations of fluid-filled crack damage in slabs to produce novel predictions of the effects of dehydration on the seismology of subduction zones. These predictions have major implications for current models of supra-subduction zone seismic anisotropy, mantle flow patterns and potentially for the nucleation of intraslab earthquakes. In addition, our findings add a new dimension to the existing evidence, based largely on work in crustal rocks, for a strong coupling between metamorphic reaction, brittle fractures and fluid flow.

2. Metamorphic fluids, dehydration reactions and fractures

2.1 Metamorphism, fluids and fractures

The involvement of a free fluid phase in metamorphic reactions and its movement through various scales of fracture have been extensively documented (Etheridge et al., 1984; Oliver, 1996), and the physical mechanisms have been explored with numerical models (Connolly, 1997; Simpson, 1999). The focus of this previous work has been on regional metamorphism within the continental crust. Hydration of oceanic crust and lithosphere occurs at mid-ocean ridges, along transform faults and at outer rise faults before the slab is subducted (Peacock, 1990), and is incorporated into the lattice structure of new hydrous minerals. Subduction of

such hydrated oceanic slab rocks means that dehydration reactions will be important (Peacock, 1993; Pawley & Holloway, 1993; Schmidt & Poli, 1998; Hacker et al., 2003a).

2.2 Dehydration reactions, volume changes and pressure

The mechanical consequences of dehydration have been extensively documented, again mainly in the context of the continental crust (e.g. Hacker, 1997; Wong et al., 1997; Simpson, 1999), but see Miller et al. (2003) for a study applied to subduction zones. As dehydration proceeds and a free fluid phase is evolved, the key factor influencing the bulk mechanical response is how, or whether, this fluid is accommodated by the host rock. The relative volumes of the reactants and reaction products (solid and fluid) are important (Hacker, 1997), but so also is the deformation of the matrix framework (Wong et al., 1997). If the host rock matrix deforms quickly enough by compaction or creep and there exists a low pressure or 'drained' boundary to the rock volume undergoing reaction, then the pore fluid pressure will remain low and the reaction will proceed (Hacker, 1997; Wong et al., 1997). However, if the host rock matrix cannot deform quickly enough with respect to the dehydration rate and the boundaries of the reacting volume are sealed, or 'undrained', then the pore fluid pressure can rise and exceed the confining pressure, and the dehydration reaction may slow or even stop (Hacker, 1997; Wong et al., 1997). In this 'undrained' case, the pore fluid pressure is limited only by the value of the minimum compressive stress plus the tensile strength of the rock (Phillips, 1972).

A further important point is that in a dynamic system such as a descending slab, as hydrated rocks are constantly being delivered to the 'dehydration window', new dehydration reaction sites will be forming all the time. At the instant of initiation, any newly formed pore will contain a pore fluid at a fluid pressure at least equal to the confining pressure, before any

connectivity can drain this fluid away. There is a constant supply of new 'undrained' pores as undehydrated rocks are passed through the 'dehydration window'. The key issues relating to the mechanical effects of a fluid produced by dehydration reactions at slab conditions (P ~10^2-10^3 MPa, T ~10^2 °C), are both spatial and temporal. What is the geometry and distribution of the fluid phase? Over what timescale does this fluid evolve and move?

2.3. Dehydration-induced fluid-filled cracks in subducted rocks

2.3.1 Evidence for a discrete, mobile fluid phase in subducting slabs

Two simple end-member models for the geometry of the fluid produced by dehydration reactions are:

1. a grain boundary 'film', structured or polarised by neighbouring grains, and probably very thin i.e. on the order of several atomic distances across.

2. a discrete fluid phase located within inequant pores, cracks, fractures and veins, from the scale of intergranular grain boundary cracks to transgranular fractures and veins, i.e. many atomic distances across. Note that any pores are likely to be inequant because dehydrating slab rocks will be subject to a deviatoric stress, and will likely have macroscopic foliations defined by shape preferred orientations of grains – porosity in these rocks is defined by inequant pores with high aspect ratios.

Many studies of previously subducted rocks document the former existence of a discrete fluid phase in fractures, cracks and veins. Field examples of exhumed high pressure (HP) and ultra-high pressure (UHP) rocks commonly preserve prograde mineral assemblages in brittle veins cross-cutting ductile fabrics. Eclogitic veins in blueschist- and amphibolite-facies host rocks

have been reported from various localities in the Western Alps (Philippot, 1987; Pennacchioni, 1996), New Caledonia (Spandler & Hermann, 2006) and Tianshan (John et al., 2008). In these examples, fluid inclusions attest to the presence of a free fluid phase, crack-seal vein fill geometries demonstrate cyclic variations in pore fluid pressure and euhedral crystals show that some crystal growth occurred in cavities even at these elevated pressures. Field evidence from the Voltri massif in Italy shows multiple generations of prograde veins, both deformed and undeformed, suggesting a cyclic process of fluid production and associated fracture contemporaneous with ductile deformation (Scambelluri et al., 1995; Hermann et al., 2000).

Laboratory experiments conducted at pressure (P) and temperature (T) conditions relevant to slabs and on likely slab lithologies also document dehydration-induced cracking. Hirose et al. (2006) performed torsion experiments on dehydrating serpentinite (lizardite, P = 0.3-0.4 GPa, T = 550-650°C). The shear deformation produced a foliation from the originally random texture and dehydration-induced brittle cracks cut across this foliation at ~45°. Jung et al. (2004) produced dehydration embrittlement of antigorite serpentinite at higher pressures (P = 1-6 GPa, T = 550-820°C), with macroscopic shear fractures and many smaller cracks. Tenthorey and Cox (2003) found that permeability rose rapidly and then levelled off once dehydration started in antigorite serpentinite (P = 300 MPa, T = 600-700°C). Dobson et al. (2002) also produced dehydration embrittlement just above the dehydration temperature of antigorite serpentinite marked by acoustic emissions (P = 1.5-8.5 GPa, T = 300-900°C) and thin sections showing brittle cracks normal to the local minimum compression. Rutter and Brodie (1988) produced shear fractures decorated with fine grained olivine (i.e. a reaction product) during the dehydration of serpentinite (P = 0.1-0.3 GPa, T = 300-600°C). These shear fractures formed through the interaction and coalescence of tensile microcracks. Murrell and Ismail (1976) performed axial tests on partially serpentinised (antigorite) peridotite, with a

pre-existing foliation ($P \leq 0.55$ GPa, $T \leq 670$°C). At temperatures above the dehydration reaction, the samples failed in shear fractures at low strength.

2.3.2 Evidence for a persistent fluid phase in subducting slabs

In a dynamically deforming and reacting system such as a subducting slab, any single pore or crack could be highly transient and short-lived. However, a section of hydrated slab will dehydrate over a finite interval of time, and fluid will be evolved over this interval. For slabs descending at rates of centimetres per year, this time will be short in geological terms, but for seismic frequencies of several Hertz, this is a very long time. In addition, at any given time, a large volume of rock in the slab is actively dehydrating and therefore there will always be a large number of open fluid-filled cracks, pores and veins as the subduction process continuously supplies more hydrated rock. As each dehydrated section descends, a new section of the slab enters the 'dehydration window' and starts producing fluid. Even though specific dehydration reactions are discontinuous or pulsed over time, there are many hydrous phases (Mainprice & Ildefonse, 2008) and numerous dehydration reactions (Pawley & Holloway, 1993; Schmidt & Poli, 1998; Hacker et al., 2003a). For a given depth, fluid production will be quasi-continuous, forming new cracks, re-opening old ones and closing others.

The crack-seal vein textures reported in many of the HP veins listed above further support the notion that fluid-induced tensile failure is cyclic and sustained. The concentration of solutes such as Al, Si, Na, and Ca in aqueous fluids from dehydration reactions in slabs is very low (Manning, 2004). Therefore, the cyclic crack-seal growth of a vein measuring several cm in thickness requires a sustained fluid flux over time of approximately constant composition. Further evidence for a persistent, mobile fluid phase in slabs comes from the

mantle wedge overlying the slab. Chemical data show that hydrous fluids derived from the slab metasomatise the wedge and may trigger partial melting (Bebout, 1991; McInnes et al., 2001). To move a hydrous fluid from the slab into the wedge requires a combination of fluid production in the slab from dehydration reactions and movement of this fluid through the slab and into the mantle wedge (i.e. permeability, connected porosity). Seismological evidence from Chile suggests that the rate of this fluid flux is far in excess of that possible along thin grain boundary films, and that advective transport in fractures is much more likely (Nippress & Rietbrock, 2007).

2.4 Summary of existing evidence

Fluid-filled cracks in an 'undrained', or slowly draining matrix cannot close instantaneously, even at high confining pressures. The bulk modulus of water is high enough (2-3 GPa, allowing for a fraction of dissolved CO_2) to prevent total crack or pore closure. This is at odds with the commonly held view that *all* cracks close with increasing confining pressure, which has arisen principally from the results of dry experiments and experiments without reactions (e.g. Kern, 1993). Many field observations, experimental studies and theoretical analyses suggest that a macroscopic, mobile and quasi-continuously produced fluid phase exists in slabs during subduction. In this paper, we present new field and microstructural data that demonstrate the existence of this fluid phase during the subduction of slabs in the Western Alps (Section 3) and assess the links between specific dehydration reactions and brittle fractures (Section 4) and the implications for seismic velocity anisotropy (Section 5).

>>> Figure 1 about here

3. Field observations from exhumed slabs in the Western Alps

3.1 Blueschist to eclogite dehydration in oceanic crust – evidence from Salicetu, Schistes Lustres unit, Alpine Corsica

Samples of blueschist metabasalt were collected from around Salicetu (UTM 32T 524332E 4694196N, using datum WGS84) in Alpine Corsica (Figure 1). The remnants of a subducted oceanic slab have been exhumed to the surface along extensional faults, some of which may reactivate former subduction thrusts (Jolivet et al., 1990). Peridotites and gabbros from the mantle portion of this former slab preserve evidence for subduction seismicity as pseudotachylytes that devitrified at blueschist facies conditions (Austrheim & Andersen, 2004). Peak conditions for the prograde metamorphism in the slab reached lawsonite eclogite facies with P = 1-1.4 GPa, T = 420°C (Figure 2; Caron & Pequignot, 1986), although much of the exposed rock preserves blueschist facies assemblages.

>>> Figure 2 about here

Blueschist metabasalts locally have a strong planar fabric defined by aligned glaucophane (Figure 3). Veins of eclogite facies minerals (omphacite, garnet, lawsonite, phengite and carbonate) are abundant, and vary in thickness from mm to several cm, and extend up to tens of cm in length. The majority of these eclogitic veins now lie parallel to the blueschist foliation and show a mineral stretching lineation, but some clearly cross-cut the fabric (Figure 3a, b). These relationships document an extended history of brittle eclogitic vein formation synchronous with ductile fabric development in the host blueschists. The veins

have sharp margins, and clearly indicate a brittle fracture origin, rather than segregation by diffusive mass transfer (Figure 3c). The fibrous habit of omphacite, with crystal fibres oriented approximately normal to the vein margins is also consistent with growth from a free fluid phase within a brittle fracture (Figure 3d).

>>> Figure 3 about here

From the limited exposures at Salicetu it is unclear whether the vein fluids were sourced in situ or whether the veins represent advective channels (e.g. John et al., 2008). Nevertheless, discordant and concordant eclogitic veins in blueschist metabasalts in Corsica document dehydration-induced cracking in the upper part of a subducting oceanic slab, overlapping with ductile deformation producing the foliation. Fluid-filled cracks formed in orientations oblique to the host blueschist fabric, and crystallised vein-filling minerals at eclogite facies conditions.

3.2 Serpentinite dehydration in the mantle – Erro-Tobbio, Voltri massif, Italy

A further suite of samples has been recovered from the Erro-Tobbio (UTM 32T 485360E 4934252N) region of NE Italy (Figure 1). The dominantly ultrabasic rocks in this area are derived from sub-continental mantle, and were initially exhumed at the sea floor, then subducted during the Alpine orogeny and finally exhumed (Hermann et al., 2000). Hoogerduijn-Strating & Vissers (1991) assigned serpentinite mylonites to different stages of the prograde and retrograde path in this history based on kinematic indicators and syntectonic mineral assemblages with respect to the local matrix. Olivine bearing assemblages

have been reported in veins, and the vein formation has been linked with shear in the mylonites. These authors assert that plastic deformation at eclogite facies occurred simultaneously with crack propagation, shear fracturing and deposition of the olivine vein assemblages.

In detail, many of the veins cutting the mylonitic foliation in antigorite serpentinites contain a coarse, often fibrous, assemblage of olivine, Ti-rich clinohumite, diopside and magnetite. This vein assemblage represents a prograde dehydration with respect to the host rock (Scambelluri et al., 1995). Metamorphic conditions have been estimated at P = 2-2.5 GPa and T = 550-600°C, i.e. eclogite facies (Figure 2; Messiga et al., 1995). Prograde olivine veins occur in the serpentinite mylonites, which localised most of the subduction deformation, and the peridotite wall rocks of these mylonites. Dehydration reactions generating olivine from serpentinite affected all parts of the down going slab, and not just the localised serpentinite shear zones (Scambelluri et al., 1991).

>>> Figure 4 about here

In the bed of the Gorzente river, olivine-bearing veins are locally abundant and, in the undeformed state, vary in thickness from mm to several cm, and extend laterally for several m (Figure 4a). Some veins are sheared, rotated and folded into the foliation in the host serpentinite (Figure 4b). Undeformed veins are typically sub-horizontal and oriented at ~45° to the intense mylonitic fabric (Figure 5a, b, c). The opening vector of the veins, recorded by the vein fibres and matching dilatational jogs, is sub-parallel to a stretching lineation defined by elongate antigorite clusters lying in the foliation of the host serpentinite (Figure 5d). The evidence for these veins filling brittle fractures is overwhelming, and includes sharp, planar

283 sides; matching asperities in the separated vein walls; curved horn-like tips and frequent
284 branching apophyses (Figure 6). The fibrous nature of the vein-filling minerals, with fibres
285 oriented normal to the margins supports crystal growth in veins, rather than segregation in
286 the solid state (Figure 6a). These observations further support the hypothesis that brittle
287 fracture formation, fluid production, crystallisation of dehydration products in the veins and
288 ductile deformation in the host serpentinite mylonite were coeval and kinematically linked.
289 The prograde olivine bearing veins in the serpentinite mylonites of the Erro-Tobbio region
290 document a coupled system of dehydration-induced cracking, vein formation and plastic
291 deformation occurring in mylonites located in the mantle portion of a subducting slab. The
292 combination of undeformed (cutting the host serpentinite fabric) and deformed (folded or
293 concordant with the fabric) olivine bearing veins attests to an extended period of
294 dehydration-induced fracture, synchronous with ductile deformation in the enclosing
295 serpentinite mylonites.

296

297 >>> Figure 5 about here

298 >>> Figure 6 about here

299

300 **4. Hydrofracture and dehydration reaction**

301

302 For the estimated *P*, *T* conditions (Caron & Pequignot, 1986), a simplified dehydration
303 reaction (assuming an Fe-free system) for the blueschist metabasalts at Salicetu is:

304

305 $$4\ Gln + 3\ Lws = 8\ Jd + 3\ Prp + 3\ Di + 7\ Qtz + 10\ H_2O$$

306

307 which generates an eclogitic mineral assemblage in the veins (Evans, 1990). For the antigorite
308 serpentinites at Erro-Tobbio, a possible reaction (Scambelluri et al., 1991) is:

309

310 $$1\ Atg + 20\ Brc = 34\ Fo + 51\ H_2O$$

311

312 which accounts for the prograde olivine in these veins. Using molar volume data from Holland
313 & Powell (1998), we calculate the changes in solid (ΔV_s) and fluid (ΔV_f) volume, and then the
314 total volume change for these reactions (ΔV_{rxn}), following the methods of Nishiyama (1989)
315 and Hacker (1997). For the blueschist reaction, at P = 1.4 GPa and T = 420°C, the values are:

316

317 $\Delta V_s = -12.1\%$

318 $\Delta V_f = +12.4\%$

319 $\Delta V_{rxn} = +0.3\%$

320

321 and for the serpentinite reaction at eclogite facies conditions (P = 2 GPa, T = 650°C), the
322 values are:

323

324 $\Delta V_s = -41.9\%$

325 $\Delta V_f = +47.0\%$

326 ΔV_{rxn} = +5.1%

327

328 It is clear from these calculations, and more generally from the steep to slightly negative
329 slopes of the reaction lines (Figure 2), that total volume changes are small. The dominant term
330 in the calculation of volume changes is that of the molar volume of water (i.e. minerals are
331 nearly incompressible), and this decreases markedly at elevated *P* and *T*. Quantitative data on
332 the tensile strengths of these rocks at these pressures and temperatures are lacking, but we
333 infer that the predicted volume changes of these reactions, while small, are sufficient to drive
334 *in situ* hydrofracture of these rocks.

335 Our field and microstructural evidence clearly demonstrate that brittle hydrofractures
336 must have formed at these conditions, i.e. that pore fluid pressure exceeded the local
337 minimum compressive stress + tensile strength. In the analysis by Hacker (1997), which
338 focussed on reactions in fault zones due to seismically induced pressure changes, compaction
339 of the matrix and the consequences for porosity were not considered. Under subducting slab
340 conditions, deviatoric stress will likely compact any 'excess' porosity and cause the pore fluid
341 pressure to rise. Data from reaction kinetics for relevant rocks at these conditions are rare,
342 despite the importance of the relative rates of fluid production (reaction rate) and compaction
343 creep (Wong et al., 1997). The kinetics of an antigorite dehydration reaction have been
344 measured experimentally by Perrillat et al. (2005), and they have shown that water
345 production rates of 10^{-6} to 10^{-8} s^{-1} could exceed deformation by ductile mechanisms, such as
346 compaction creep, which is typically in the range 10^{-12} to 10^{-14} s^{-1}, although in these
347 experiments there was no control on the activity of water.

348 Rock deformation experiments designed to include serpentinite dehydration show that
349 under deviatoric stress and 'undrained' conditions (constant pore fluid volume), pore fluid

pressure rises and leads to dehydration embrittlement (Raleigh & Paterson, 1965; Dobson et al., 2002; Jung et al., 2004). However, for 'drained' (constant pore fluid pressure) conditions, the porosity created by dehydration is reduced and the fluid is forced to move elsewhere (Rutter & Brodie, 1988; Rutter et al., 2009). The field and microstructural evidence from naturally deformed rocks supports the idea that ductile deformation of the matrix, dehydration reactions and brittle fracture all overlapped in space and time. Rutter et al. (2009) have suggested that fluids expelled from actively dehydrating and compacting serpentinite will migrate to stronger units and cause these to fail seismogenically. The evidence described above suggests that this sequence of dehydration, fluid migration and brittle failure can occur within the same lithological unit. In this scenario, only localised volumes of antigorite serpentinite (Erro-Tobbio) or blueschist (Corsica) undergo dehydration and compaction at any one time, and the fluid produced migrates locally, most probably up-dip (up-slab), and produces hydrofractures in stronger non-dehydrating rock volumes of the same composition. This is consistent with trace element and isotopic data, that shows that fluids in dehydrating slabs are locally sourced and in equilibrium with the wall rocks (Scambelluri & Philippot, 2001).

5. Modelling intra-slab anisotropy

5.1 Background and rationale

Elastic anisotropy in rocks generates azimuthal variations in longitudinal (P) wave velocity V_p (Hess, 1964) and shear (S) wave splitting (Mainprice & Silver, 1993), measured by the azimuth of fast S wave polarisation (ϕ, hereafter the "fast axis"), the delay time between the arrivals of fast (S_1) and slow (S_2) shear waves (δt), and the azimuth-dependent difference in

374 the shear wave velocities (δV_s). Hydrous phases such as amphibole and serpentine are
375 intrinsically anisotropic in their elastic properties (Mainprice & Ildefonse, 2008; Tatham et al.,
376 2007), and also display mechanical anisotropy favouring their growth and rotation into
377 parallelism with the rock fabric in the deforming slab. Aligned hydrous minerals thereby add
378 elastic anisotropy to the bulk rock aggregate, until the slab reaches a depth (> ~100 km)
379 where dehydration reactions generate a dominantly anhydrous mineral assemblage.

380 Our field evidence, taken with the wealth of previous field and experimental
381 observations, demonstrates that at any given instant (i.e. over the timescale of a seismic wave
382 train), there will be a large population of fluid-filled cracks in the slab, and that this
383 dehydration-induced damage occurs in slabs to depths of at least 100 km. These fluid-filled
384 cracks form oblique (~45°, Figure 5) to strong slab-parallel ductile fabrics and are therefore
385 sub-horizontal in the slab. Dehydration reactions in the hydrated portion of the slab are quasi-
386 continuous (Hacker et al., 2003a), generating new fluid-filled cracks as previously formed
387 veins crystallise and deform. At the time scale of seismic waves propagating across the slab
388 with a frequency of several Hz, sub-horizontal fluid-filled cracks exist in the dehydrating
389 layers, and will influence the passing seismic energy, either teleseismic or locally sourced in
390 the slab. This is highly significant because systematic patterns of fluid-filled cracks provide an
391 additional component of elastic anisotropy compared to intact rocks, and can modify P wave
392 anisotropy and S wave splitting (Crampin, 1981). The contribution of the solidified veins to
393 the seismic anisotropy has not been modelled, as their elastic properties will be almost
394 identical to those of the host matrix, especially in comparison to the contrast in stiffness
395 produced by fluid-filled cracks.

396

397 *5.2 Modelling the elastic anisotropy of slab rocks*

398 The practicality of using laboratory measurements of velocity anisotropy for slab rocks is
399 complicated by both the extreme conditions (of *P*, *T* and stress, σ) and the frequency
400 dependence of elastic response in saturated rocks. Ultrasonic laboratory measurements of
401 velocities are conducted in the range of MHz, whereas the *in situ* seismic response is in the Hz
402 to kHz range. The elastic response, measured in terms of the compliances or stiffnesses, is
403 very different in these two cases, and there is no simple extrapolation of ultrasonic laboratory
404 velocity measurements to the seismic velocities of rocks in situ (Guéguen & Sarout, 2009). To
405 explore the influence of saturated crack damage on the seismic response of slab rocks we
406 calculate the elastic properties of mineral aggregates using a rock recipe approach (Tatham et
407 al., 2007), and then add saturated crack damage using expressions from Effective Medium
408 Theory (EMT; Guéguen & Sarout, 2009). The elastic properties predicted for damaged rocks,
409 in both dry and saturated states, have been validated against detailed experimental data for a
410 range of lithologies and crack damage patterns (Schubnel et al., 2006; Katz & Reches, 2004;
411 Sarout et al, 2007). For seismic wavelengths (frequencies), the appropriate formulation from
412 EMT is for the saturated and relaxed state, or low frequency approximation (Guéguen &
413 Sarout, 2009).

414 We calculate the elastic properties of two equilibrium mineral assemblages in the slab,
415 one for the oceanic crust based on a wet basalt protolith and one for the oceanic mantle
416 derived from a wet harzburgite protolith (Hacker et al., 2003a). Modal proportions are
417 calculated for *P*, *T* conditions at 75 km depth in the slab of an old and relatively cold
418 subduction zone (e.g. beneath present day Honshu, Japan), and these generate a blueschist
419 and a serpentinite for comparison with our field data from Corsica and Erro-Tobbio,
420 respectively (see Section 3). From the modal data listed in Hacker et al. (2003a, their table 3),
421 not all of the phases have published elasticity data, so the following substitutions were made:
422 all antigorite mapped to lizardite, all amphiboles to hornblende, all accessory phases to

quartz. The depth interval over which dehydration reactions occur is a complex function of slab temperature, chemical composition and the volume of water incorporated before subduction (Hacker et al., 2003a; Mainprice & Ildefonse, 2008). Over the finite depth range where the dehydration occurs, the elastic (and seismic velocity) anisotropy of each rock in the slab will be a mixture of plastic (LPO) and brittle (crack damage) components.

To calculate the LPO component of the elasticity tensor for each rock, we assumed the foliation is perfectly parallel and the lineation is down-dip. Note that because of this assumption, i.e. perfect alignment of all mineral phases with the fabric, our predictions of intact rock anisotropy are upper bounds. Details of the mapping between mineral crystallographic axes and fabric axes are listed in Table 1. We used published elastic properties for single minerals at ambient *P* and *T*, because complete data for the *P, T* dependence of the elasticity properties of all minerals used in this study are not yet available. Measurements from deformation experiments on mantle rocks suggests that the mutually antagonistic effects of *P* and *T* on seismic velocity effectively cancel each other out (Kern, 1993). Elastic stiffness tensors are calculated for the bulk rock aggregate from single mineral elastic constants and our selected crystallographic orientations using standard methods (Mainprice, 1990). To calculate the effect of fluid-filled crack damage on the elastic compliance of the intact rocks, we assumed parallel cracks oriented at 45° to the original LPO and used the saturated, low frequency (undrained) approximation valid for seismic frequencies (Hz to kHz). Compliances of saturated damaged rocks are calculated with a bulk modulus of water of 3 GPa and a crack aspect ratio of 0.001 using expressions in Guéguen & Sarout (2009). We inverted the compliance tensor to obtain the elastic stiffness.

5.3 Model results

447

448 *5.3.1 Seismic velocity anisotropy of intact blueschist and serpentinite*

449 For the intact rocks with no dehydration damage, the predicted magnitude and azimuthal
450 variation of V_p and δV_s are broadly similar to dry experimental measurements made at
451 elevated *P* and *T* (Figures 7 and 8; Kern, 1993). Our modelled values (percentages on Figures
452 7 and 8) are higher than those measured in the laboratory partly because the modelled
453 mineral alignments are perfect within the bulk rock fabric. Note also that laboratory
454 measurements of velocities in dry rocks using ultrasonic frequencies (MHz) cannot in general
455 be used for the seismic response (Hz) in situ (Guéguen & Sarout, 2009). Seismic velocity
456 anisotropy is known to be extremely high for rocks dominated by hydrous sheet silicates,
457 reaching 70% for serpentinite (Figure 8), reflecting the contribution of the dominant hydrous
458 minerals (Mainprice & Ildefonse, 2008). V_p anisotropy is dominated by maxima oriented
459 trench-normal and down-dip of the slab for the blueschist (Figure 7a) and more uniformly
460 within the plane of the slab for the serpentinite (Figure 8a). The predicted S wave splitting
461 anisotropy (δV_s, Figure 7b, Figure 8b) is also very high compared to average mantle values of
462 3 – 7% (Mainprice & Silver, 1993).

463

464 >>> Figure 7 about here

465

466 *5.3.2 Seismic velocity anisotropy of damaged blueschist and serpentinite*

467 For damaged rocks with sub-horizontal fluid-filled cracks from dehydration reactions, the V_p
468 maximum is rotated away from a trench-normal orientation to a trench-parallel orientation
469 for both the blueschist (Figure 7d) and the serpentinite (Figure 8d), and the magnitude of

maximum V_p anisotropy remains very high. Another significant effect of the composite anisotropy produced by the interaction of the brittle crack damage with the ductile LPO is on the shear wave splitting. The magnitude of splitting (δV_s) increases in the damaged blueschist, even for low crack densities (e.g. 0.1, Figure 7e), and remains high in the damaged serpentinite (Figure 8e). Importantly, the fluid-filled crack damage rotates the polarization direction of the fast S wave (S_1) to produce very significant changes in ϕ. For S waves propagating exactly in the vertical plane, the shear wave splitting is zero (Figure 7e,h; Figure 8e, h). However, for S waves propagating at steep angles (but not truly vertical) through these slab rocks, the polarisation direction of S_1 is predicted to rotate from trench-normal to trench-parallel (Figure 7f, i; Figure 8f, i).

When a parallel crack pattern is added to an oblique LPO the resulting elastic anisotropy has a broadly monoclinic symmetry, with the fast V_p direction now parallel to the intersection of the crack planes and the foliation. For the case of a subducting plate with a slab-parallel LPO and down-dip lineation, the addition of sub-horizontal crack planes produces a sub-horizontal intersection oriented parallel to the trench. This interaction between the plastic LPO of aligned minerals and the brittle fabric of dehydration-induced cracks rotates the V_p maximum and the S_1 polarization azimuth (ϕ) for non-vertical rays from trench-normal to trench-parallel. This predicted rotation of the V_p maximum direction is consistent with recent observations from the slab beneath Japan (Ishise & Oda, 2005).

>>> Figure 8 about here

5.4 Delay times from anisotropic rocks in the slab

493 The effects of intraslab anisotropy on delay time (δt) has been estimated by integrating the
494 predicted anisotropy over the path traversed by a propagating S wave. Work in progress by
495 the authors aims to document and quantify the geometry of anisotropy in previously
496 subducted slab rocks, including components from foliations (LPOs) and crack damage
497 (dehydration-induced veins). In the absence of empirical field measurements, we can make
498 qualified assumptions about the likely distributions and thicknesses of different rock types,
499 their fabrics and the role of crack damage, to estimate their contribution to intraslab seismic
500 anisotropy.

501 We assume an original oceanic crust ~7 km thick for an old and cold slab, with a
502 MORB composition (basalt, dolerite, gabbro) completely metamorphosed to blueschist at 75
503 km depth, and ~1 km of serpentinite beneath this formed from metamorphosed hydrated
504 harzburgite. For a slab dipping at 30°, 8 km true thickness maps to 9.2 km vertical thickness.
505 This will be the distance travelled across this top portion of the slab for a locally sourced S
506 wave starting at the base of the serpentinite, a plausible source region for intraslab seismicity.
507 The equation for the delay time is (Mainprice & Silver, 1993):

508

509 $$\delta t = h * \delta V_s / V_{s\_avg}$$

510

511 where h is the distance travelled by the S wave through the anisotropic slab, δV_s is the
512 dimensionless S wave anisotropy in the direction of propagation and V_{s_avg} is the average of S
513 wave velocities (= $(V_{smax} - V_{smin})/2$). Note that Figures 7 and 8 show that S waves propagating
514 in a perfectly vertical direction will not be split, only waves propagating 10°-20° from the
515 vertical. In fact, the vast majority of S waves recorded at the surface in the forearc will not
516 have travelled vertically through the slab. Steep but non-vertical S waves will pass through a

517 thicker section of the slab anisotropy compared to a vertical wave, and therefore 'see' more of
518 the anisotropy. We model this as 10 km total thickness and using the values of δV_S from Figure
519 7e and Figure 8e for blueschist and serpentinite with a low density of cracks, the delay times
520 are 6.8 s from the 8.5 km of blueschist and 1.35 s from the 1.5 km of serpentinite. Many
521 subduction zones display double Benioff zones with separate upper and lower seismic zones
522 within the slab (Brudzinski et al., 2007). These distinct earthquake source regions provide an
523 opportunity to test our model, as rays originating from events in the lower seismic zone
524 should traverse different strengths and thicknesses of dehydration-induced anisotropy in
525 comparison to events from the upper seismic zone.

526 In reality, many factors will combine to lower the actual delay time through the slab,
527 including: incomplete metamorphic transformation of the slab rocks; fabrics and cracks will
528 not be perfectly aligned; and the crack density will vary. All of these factors will reduce the
529 predicted magnitude of S wave splitting delay times. Our estimates serve as upper bound
530 maxima to the possible degree of anisotropy produced from within the slab. We are acutely
531 aware that the geometry of anisotropic rocks in slabs is very poorly constrained at present,
532 including the thicknesses of anisotropic units, the orientation and strength of LPOs and the
533 density of crack damage from dehydration reactions. However, our simplified calculations
534 show that the predicted magnitude of elastic anisotropy produced within the slab due to the
535 combined effects of LPOs and fluid-filled crack damage can generate measurable seismic
536 birefringence from local S wave sources, comparable to the observed values of up to 3 s
537 (Savage, 1999; Park & Levin, 2002).

538

539 >>> Figure 9 about here

540

6. Discussion

6.1 The effects of fluid-filled crack damage on the seismic anisotropy of slabs

Our models use scalar crack densities of 0.1 and 0.5, which are well below values recorded at whole rock failure (Schubnel et al., 2006; Katz & Reches, 2004). Increasing the crack density to higher values would simply produce a horizontal plane of V_p and δV_s maxima within the slab, and there would be no rotation of ϕ to trench-parallel orientations. The lower crack density value of 0.1 is approximately the lower limit for the percolation threshold (Guéguen et al., 1997). Because the magnitude of the extrinsic anisotropy produced by fluid-filled cracks generally outweighs the intrinsic anisotropy of an intact aggregate, the role of the ductile fabric in our synthetic rocks may appear superfluous. However, for low crack densities consistent with the field observations, our models show that it is the composite effect of the brittle damage with the plastic fabric that generates the significant changes in seismic anisotropy: the re-orientation of maximum V_p to trench-parallel; the maintenance of high values of δV_s for ray propagation directions at high angle to the slab; and the re-orientation of fast polarisation directions from trench-normal for intact rocks to trench-parallel for the damaged rocks. Note also that exhumed slab rocks unequivocally display strong macroscopic fabrics and lattice preferred orientations of aligned minerals. Lastly, as subduction proceeds and the progressively more anhydrous slab rocks metamorphose and recrystallise with depth, dehydration-induced damage will be annealed, and the ductile fabric in the slab reorients the seismic anisotropy with trench-normal fast axes for both P and S_1 waves (Figure 9).

6.2 Complexities of subducting slabs

564 Exhumation of a subducted slab is, by definition, atypical: most oceanic slab rocks are
565 successfully subducted into the mantle. Nevertheless, the field evidence for the former
566 presence of prograde fluid-filled cracks in these slab rocks is unambiguous. The mantle rocks
567 at Erro-Tobbio have had a complex history that has included: extensional exhumation of
568 mantle at the sea floor; subduction during the Alpine orogeny; and then extensional
569 exhumation and uplift to the surface (Scambelluri et al., 1995; Hermann et al., 2000). We also
570 note that the ductile fabrics exposed in these rocks are not in reality perfectly parallel, and the
571 dehydration-induced veins are not all perfectly parallel either. Ductile fabrics in subducting
572 slabs could well be inclined to the macroscopic boundaries of the subduction zone, and stress
573 rotations in weak deforming layers would then promote crack orientations away from
574 horizontal (Healy, 2008; In press). In the absence of a systematic, quantitative dataset of
575 measured slab fabrics and vein orientations and their distribution in the slab, we believe our
576 end-member models of perfect alignments of fabrics and cracks provide useful upper bound
577 estimates of intraslab seismic anisotropy.

578

579 **7. Summary**

580 Evidence from field data, laboratory experiments and theory confirms that down going slabs
581 dehydrate and this induces fluid-filled cracks. These cracks occur over scales of time and
582 length that are highly significant for measurements of supra-subduction seismic anisotropy.
583 Specifically, the sustained production of dehydration-induced saturated cracks over a finite
584 depth interval changes the elastic properties of the intact rock aggregate in a manner that will
585 affect the seismic energy crossing the slab.

586 Our model shows that brittle crack damage caused by dehydration reactions in the
587 descending slab combines with the anisotropy of plastically deformed and metamorphosed

588 rocks to generate fast directions of seismic velocities parallel to the slab and trench at the
589 modelled depth (75 km). Our model results predict that trench-parallel seismic fast directions
590 observed in supra-subduction forearcs can be explained by intraslab anisotropy, and that the
591 role of olivine fabrics (Type A or Type B) in relation to observed anisotropy above the mantle
592 wedge is therefore open to question.

593 A further important prediction of our model is that trench-parallel fast axes are
594 restricted to the surface area lying above the 'dehydration window' of the down going slab, i.e.
595 the depth interval over which dehydration reactions are significant. Once the slab has
596 dehydrated, further metamorphic reactions and recrystallisation will obliterate any
597 dehydration-induced crack damage and the seismic anisotropy recorded at the surface above
598 this region will be dominated by the LPO alone i.e. trench-normal fast axes, consistent with
599 the observations from back-arc regions (Nakajima & Hasegawa, 2004; Long & van der Hilst,
600 2006).

601 Our dehydration damage hypothesis for trench-parallel fast axes is supported by
602 existing field and laboratory observations of deformation in slab rocks. Consequently, we
603 believe that previous interpretations of supra-subduction seismic anisotropy based solely on
604 mantle flow directions may be flawed since they ignore the significant elastic and seismic
605 anisotropy originating within the slab. Our model has general application to any subduction
606 zone with dehydration in the slab, and does not rely on specific conditions of forearc water
607 content, stress state in the mantle wedge or complex 3D flow geometries.

608

609 **Acknowledgements**

610 DH and AVB thank Jörg Hermann and Daniela Rubatto (both at ANU) for discussion and
611 assistance in the field. All authors thank Katy Evans, Chris Clark (both at TIGeR) and Sara

612 Pozgay, Ian Jackson and Brian Kennett (all at ANU) for conference discussion (AESC Perth,
613 2008). Thanks also to Tim Holland (Cambridge) for help with molar volume data in
614 THERMOCALC. Comments on an earlier version of the manuscript by Mike Kendall (Bristol)
615 helped to clarify the arguments made in the final version. Brad Hacker (UCSB) is thanked for a
616 constructive review. Fellowships from TIGeR/Curtin University for DH and SMR, and ARC
617 grant DP0878453 are gratefully acknowledged. This is TIGeR publication 180.

618

619 **References**

620

621 Abers, G. A., van Keken, P. E., Kneller, E. A., Ferris, A. & Stachnik, J. C. 2006. The thermal
622 structure of subduction zones constrained by seismic imaging: Implications for slab
623 dehydration and wedge flow. Earth and Planetary Science Letters 241(3-4), 387-397.

624 Abramson, E. H., Brown, J. M., Slutsky, L. J. & Zaug, J. 1997. The elastic constants of San
625 Carlos olivine to 17 GPa. J. Geophys. Res 102(6), 12253–12263.

626 Ahrens, T. J. 1995. Mineral physics & crystallography: a handbook of physical constants.
627 American Geophysical Union, Washington, DC.

628 Austrheim, H. & Andersen, T. B. 2004. Pseudotachylytes from Corsica: fossil earthquakes
629 from a subduction complex. Terra Nova 16(4), 193-197.

630 Auzende, A. L., Pellenq, R. J. M., Devouard, B., Baronnet, A. & Grauby, O. 2006. Atomistic
631 calculations of structural and elastic properties of serpentine minerals: the case of
632 lizardite. Physics and Chemistry of Minerals 33(4), 266-275.

633 Bebout, G. E. 1991. Field-Based Evidence for Devolatilization in Subduction Zones:
634 Implications for Arc Magmatism. Science 251(4992), 413-416.

635 Birch, F. 1960. The velocity of compressional waves in rocks to 10 kilobars, Part 1. J.
636 Geophys. Res 65(4), 1083-1102.

637 Brudzinski, M. R., Thurber, C. H., Hacker, B. R. & Engdahl, E. R. 2007. Global prevalence of
638 double Benioff zones. *Science* **316**(5830), 1472.

639 Caron, J. M. & Pequignot, G. 1986. The transition between blueschists and lawsonite-bearing
640 eclogites based on observations from Corsican metabasalts. LITHOS 19(3-4), 205-218.

641 Chai, M., Brown, J. M. & Slutsky, L. J. 1997. The elastic constants of a pyrope-grossular-
642 almandine garnet to 20 GPa. Geophysical Research Letters 24(5), 523-526.

643 Collins, M. D. & Brown, J. M. 1998. Elasticity of an upper mantle clinopyroxene. Physics and
644 Chemistry of Minerals 26(1), 7-13.

645 Connolly, J. A. D. 1997. Devolatilization-generated fluid pressure and deformation-
646 propagated fluid flow during prograde regional metamorphism. Journal of Geophysical
647 Research 102(B8).

648 Crampin, S. 1981. A review of wave motion in anisotropic and cracked elastic-media. Wave
649 Motion 3, 343-391.

650 Dobson, D. P., Meredith, P. G. & Boon, S. A. 2002. Simulation of Subduction Zone Seismicity
651 by Dehydration of Serpentine. Science 298, 1407-1410.

652 Etheridge, M. A., Wall, V. J., Cox, S. F. & Vernon, R. H. 1984. High fluid pressures during
653 regional metamorphism and deformation: implications for mass transport and
654 deformation mechanisms. Journal of Geophysical Research 89(B6).

655 Evans, B. W. 1990. Phase relations of epidote-blueschists. LITHOS 25(25), 3-23.

656 Faccenda, M., Burlini, L., Gerya, T. V. & Mainprice, D. 2008. Fault-induced seismic
657 anisotropy by hydration in subducting oceanic plates. Nature 455(7216), 1097.

658 Guéguen, Y., Chelidze, T. & Le Ravalec, M. 1997. Microstructures, percolation thresholds,
659 and rock physical properties. Tectonophysics 279(1-4), 23-35.

660 Guéguen, Y. & Sarout, J. 2009. Crack-induced anisotropy in crustal rocks: Predicted dry and
661 fluid-saturated Thomsen's parameters. Physics of the Earth and Planetary Interiors.

662 Hacker, B. R. 1997. Diagenesis and fault valve seismicity of crustal faults. J. Geophys. Res
663 102, 24,459–24,467.

664 Hacker, B. R., Abers, G. A. & Peacock, S. M. 2003. Subduction factory: 1. Theoretical
665 mineralogy, densities, seismic wave speeds, and H_2O contents. J. Geophys. Res
666 108(10.1029).

667 Hacker, B. R., Peacock, S. M., Abers, G. A. & Holloway, S. D. 2003. Subduction factory: 2. Are
668 intermediate-depth earthquakes in subducting slabs linked to metamorphic dehydration
669 reactions. J. Geophys. Res 108(B1), 2030.

670 Healy, D. 2008. Damage patterns, stress rotations and pore fluid pressures in strike-slip fault
671 zones. Journal of Geophysical Research, 113, B12407, doi:10.1029/2008JB005655.

672 Healy, D. In press. Anisotropy, pore fluid pressure and low angle normal faults. *Journal of*
673 *Structural Geology*.

674 Hermann, J., Müntener, O. & Scambelluri, M. 2000. The importance of serpentinite mylonites
675 for subduction and exhumation of oceanic crust. Tectonophysics 327(3-4), 225-238.

676 Hess, H. H. 1964. Seismic anisotropy of the uppermost mantle under oceans. Nature
677 203(4945), 629-631.

678 Hirose, T., Bystricky, M., Kunze, K. & Stünitz, H. 2006. Semi-brittle flow during dehydration
679 of lizardite–chrysotile serpentinite deformed in torsion: Implications for the rheology of
680 oceanic lithosphere. Earth and Planetary Science Letters 249(3-4), 484-493.

681 Holland, T. J. B. & Powell, R. 1998. An internally consistent thermodynamic data set for
682 phases of petrological interest. Journal of Metamorphic Geology 16(3), 309-343.

683 Ishise, M. & Oda, H. 2005. Three-dimensional structure of P-wave anisotropy beneath the
684 Tohoku district, northeast Japan. J. Geophys. Res 110.

685 Jackson, J. M., Sinogeikin, S. V. & Bass, J. D. 1999. Elasticity of $MgSiO_3$ orthoenstatite.
686 American Mineralogist 84(4), 677-680.

687 Jiang, F., Speziale, S. & Duffy, T. S. 2006. Single-crystal elasticity of brucite, Mg (OH) 2, to 15
688 GPa by Brillouin scattering. American Mineralogist 91(11-12), 1893-1900.

689 John, T., Klemd, R., Gao, J. & Garbe-Schönberg, C. D. 2007. Trace-element mobilization in
690 slabs due to non steady-state fluid–rock interaction: Constraints from an eclogite-facies
691 transport vein in blueschist (Tianshan, China). LITHOS.

692 Jolivet, L., Dubois, R., Fournier, M., Goffé, B., Michard, A. & Jourdan, C. 1990. Ductile
693 extension in alpine Corsica. Geology 18(10), 1007-1010.

694 Jung, H., Green, H. W. & Dobrzhinetskaya, L. F. 2004. Intermediate-depth earthquake
695 faulting by dehydration embrittlement with negative volume change. Nature, v. 428.

696 Jung, H. & Karato, S. 2001. Water-Induced Fabric Transitions in Olivine. Science 293, 1460-
697 1463.

698 Katayama, I. 2009. Thin anisotropic layer in the mantle wedge beneath northeast Japan.
699 *Geology* **37**(3), 211-214.

700 Katz, O. & Reches, Z. 2004. Microfracturing, damage, and failure of brittle granites. J. Geophys.
701 Res 109.

702 Kern, H. M. 1993. Physical properties of crustal and upper mantle rocks with regards to
703 lithosphere dynamics and high pressure mineralogy. Physics of the Earth and Planetary
704 Interiors 79(1-2), 113-136.

705 Kneller, E. A. & van Keken, P. E. 2007. Trench-parallel flow and seismic anisotropy in the
706 Mariana and Andean subduction systems. Nature 450(7173), 1222-5.

707 Kneller, E. A., van Keken, P. E., Karato, S. & Park, J. 2005. B-type olivine fabric in the mantle
708 wedge: Insights from high-resolution non-Newtonian subduction zone models. Earth and
709 Planetary Science Letters 237(3-4), 781-797.

710 Long, M. D. & van der Hilst, R. D. 2006. Shear wave splitting from local events beneath the
711 Ryukyu arc: Trench-parallel anisotropy in the mantle wedge. Physics of the Earth and
712 Planetary Interiors 155(3-4), 300-312.

713 Long, M. D. & Silver, P. G. 2008. The Subduction Zone Flow Field from Seismic Anisotropy:
714 A Global View. Science 319(5861), 315.

715 Lowman, J. P., Pinero-Feliciangeli, L. T., Kendall, J. M. & Shahnas, M. H. 2007. Influence of
716 convergent plate boundaries on upper mantle flow and implications for seismic
717 anisotropy. Geochemistry Geophysics Geosystems 8(8).

718 Mainprice, D. 1990. A FORTRAN program to calculate seismic anisotropy from the lattice
719 preferred orientation of minerals. Computers & Geosciences 16(3), 385-393.

720 Mainprice, D. & Silver, P. G. 1993. Interpretation of SKS-waves using samples from the
721 subcontinental lithosphere. Physics of the Earth and Planetary Interiors 78, pp 257-280.

722 Mainprice, D., Le Page, Y., Rodgers, J. & Jouanna, P. 2008. Ab initio elastic properties of talc
723 from 0 to 12 GPa: Interpretation of seismic velocities at mantle pressures and prediction
724 of auxetic behaviour at low pressure. Earth and Planetary Science Letters 274(3-4), 327-
725 338.

726 Mainprice, D. & Ildefonse, B. In press. Seismic anisotropy of subduction zone minerals -
727 contribution of hydrous phases. In: Subduction Zone Dynamics. Frontiers in Earth
728 Sciences. Springer.

729 Manning, C. E. 2004. The chemistry of subduction-zone fluids. *Earth and Planetary Science*
730 *Letters* **223**(1-2), 1-16.

731 Mao, Z., Jiang, F. & Duffy, T. S. 2007. Single-crystal elasticity of zoisite Ca2Al3Si3O12 (OH)
732 by Brillouin scattering. American Mineralogist 92(4), 570.

733 McInnes, B. I. A., Gregoire, M., Binns, R. A., Herzig, P. M. & Hannington, M. D. 2001. Hydrous
734 metasomatism of oceanic sub-arc mantle, Lihir, Papua New Guinea: petrology and
735 geochemistry of fluid-metasomatised mantle wedge xenoliths. *Earth and Planetary Science*
736 *Letters* **188**(1-2), 169-183.

737 Mehl, L., Hacker, B.R., Hirth, G. & Kelemen, P.B. 2003. Arc-parallel flow within the mantle
738 wedge: Evidence from the accreted Talkeetna arc, south central Alaska. Journal of Geophysical
739 Research **108**, doi: 10.1029/2002JB002233.

740 Messiga, B., Scambelluri, M. & Piccardo, G. B. 1995. Chloritoid-bearing assemblages in
741 mafic systems and eclogite-facies hydration of Alpine Mg-Al metagabbros (Erro-Tobbio
742 Unit, Ligurian Western Alps). European Journal of Mineralogy 7(5), 1149.

743 Miller, S. A., van der Zee, W., Olgaard, D. L. & Connolly, J. A. D. 2003. A fluid-pressure
744 feedback model of dehydration reactions: experiments, modelling, and application to
745 subduction zones. Tectonophysics 370(1-4), 241-251.

746 Murrell, S. A. F. & Ismail, I. A. H. 1976. The effect of decomposition of hydrous minerals on
747 the mechanical properties of rocks at high pressures and temperatures. Tectonophysics
748 31(3-4), 207–235.

749 Nakajima, J. & Hasegawa, A. 2004. Shear-wave polarization anisotropy and subduction-
750 induced flow in the mantle wedge of northeastern Japan. Earth and Planetary Science
751 Letters 225(3-4), 365-377.

752 Nippress, S. E. J. & Rietbrock, A. 2007. Seismogenic zone high permeability in the Central
753 Andes inferred from relocations of micro-earthquakes. Earth and Planetary Science
754 Letters 263(3-4), 235-245.

755 Nishiyama, T. 1989. Kinetics of hydrofracturing and metamorphic veining. Geology 17(12),
756 1068-1071.

757 Oliver, N. H. S. 1996. Review and classification of structural controls on fluid flow during
758 regional metamorphism. Journal of Metamorphic Geology 14(4), 477-492.

759 Park, J. & Levin, V. 2002. Seismic Anisotropy: Tracing Plate Dynamics in the Mantle.
760 Science 296(5567), 485-489.

761 Pawley, A. R. & Holloway, J. R. 1993. Water Sources for Subduction Zone Volcanism: New
762 Experimental Constraints. Science 260(5108), 664-667.

763 Peacock, S. A. 1990. Fluid Processes in Subduction Zones. Science 248(4953), 329-337.

764 Peacock, S. M. 1993. The importance of blueschist--> eclogite dehydration reactions in
765 subducting oceanic crust. Bulletin of the Geological Society of America 105(5), 684-694.

766 Pennacchioni, G. 1996. Progressive eclogitization under fluid-present conditions of pre-
767 Alpine mafic granulites in the Austroalpine Mt Emilius Klippe (Italian Western Alps).
768 Journal of Structural Geology 18(5), 549-561.

769 Perrillat, J. P., Daniel, I., Koga, K. T., Reynard, B., Cardon, H. & Crichton, W. A. 2005. Kinetics
770 of antigorite dehydration: A real-time X-ray diffraction study. Earth and Planetary Science
771 Letters 236(3-4), 899-913.

772 Philippot, P. 1987. Crack seal vein geometry in eclogitic rocks. Geodinamica Acta 1(3),
773 171-181.

774 Phillips, W. J. 1972. Hydraulic fracturing and mineralization. Journal of Geological Society
775 128(4), 337.

776 Raleigh, C. B. & Paterson, M. S. 1965. Experimental deformation of serpentinite and its
777 tectonic implications. J. Geophys. Res 70(16), 3965–3985.

778 Rutter, E. H. & Brodie, K. H. 1988. Experimental syntectonic dehydration of serpentinite
779 under conditions of controlled pore water pressure. Journal of Geophysical Research
780 93(B5).

781 Rutter, E.H., Llana-Funez, S. & Brodie, K.H. 2009. Dehydration and deformation of intact
782 cylinders of serpentinite. Journal of Structural Geology 31, pp 29-43.

783 Sarout, J., Molez, L., Guéguen, Y. & Hoteit, N. 2007. Shale dynamic properties and
784 anisotropy under triaxial loading: Experimental and theoretical investigations. Physics
785 and Chemistry of the Earth 32(8-14), 896-906.

786 Savage, M. K. 1999. Seismic anisotropy and mantle deformation: what have we learned
787 from shear wave splitting. Rev. Geophys 37(1), 65–106.

788 Scambelluri, M., Strating, E. H. H., Piccardo, G. B., Vissers, R. L. M. & Rampone, E. 1991.
789 Alpine olivine-and titanian clinohumite-bearing assemblages in the Erro-Tobbio peridotite
790 (Voltri Massif, NW Italy). Journal of Metamorphic Geology 9(1), 79-91.

791 Scambelluri, M., Muntener, O., Hermann, J., Piccardo, G. B. & Trommsdorff, V. 1995.
792 Subduction of water into the mantle: History of an Alpine peridotite. Geology 23(5), 459-
793 462.

794 Scambelluri, M. & Philippot, P. 2001. Deep fluids in subduction zones. LITHOS 55(1-4),
795 213-227.

796 Schellart, W. P. 2004. Kinematics of subduction and subduction-induced flow in the upper
797 mantle. J. Geophys. Res 109.

798 Schmidt, M. W. & Poli, S. 1998. Experimentally based water budgets for dehydrating slabs
799 and consequences for arc magma generation. Earth and Planetary Science Letters 163(1-
800 4), 361-379.

801 Schubnel, A., Benson, P. M., Thompson, B. D., Hazzard, J. F. & Young, R. P. 2006. Quantifying
802 Damage, Saturation and Anisotropy in Cracked Rocks by Inverting Elastic Wave Velocities.
803 Pure and Applied Geophysics 163(5), 947-973.

804 Simpson, G. D. H. 1999. Evolution of strength and hydraulic connectivity during
805 dehydration: Results from a microcrack model. Journal of Geophysical Research 104(B 5),
806 10467-10481.

807 Sinogeikin, S. V., Schilling, F. R. & Bass, J. D. 2000. Single crystal elasticity of lawsonite 85.
808 Mineral Soc America, 1834-1837.

809 Spandler, C. & Hermann, J. 2006. High-pressure veins in eclogite from New Caledonia and
810 their significance for fluid migration in subduction zones. LITHOS 89(1-2), 135-153.

811 Strating, E. H. H. & Vissers, R. L. M. 1991. Dehydration-induced fracturing of eclogite-facies
812 peridotites implications for the mechanical behavior of subducting oceanic lithosphere.
813 Tectonophysics 200(1-3), 187-198.

814 Tatham, D. J., Lloyd, G. E., Butler, R. W. H. & Casey, M. 2007. Amphibole and lower crustal
815 seismic properties. Earth and Planetary Science Letters 267, pp 118-128.

816 Tenthorey, E. & Cox, S. F. 2003. Reaction-enhanced permeability during serpentinite
817 dehydration. Geology 31(10), 921-924.

818 Wong, T. F., Ko, S. C. & Olgaard, D. L. 1997. Generation and maintenance of pore pressure
819 excess in a dehydrating system 2. Theoretical analysis. Journal of Geophysical Research
820 102, 841-852.

821

822 **Figure captions**

823

824 **Figure 1.** Location map for the new data presented in this paper. Salicetu (UTM 32T 524332E
825 4694196N, using datum WGS84) is situated in the Schistes Lustres unit of Alpine Corsica, SW
826 of Bastia. The Erro-Tobbio (UTM 32T 485360E 4934252N) region is NNW of Genoa and lies
827 within the Penninic domain of the Western Alps.

828

829 **Figure 2.** Pressure-Temperature plot showing the key reactions and estimated metamorphic
830 conditions for the two localities described in text. The antigorite reaction line is from
831 Scambelluri et al. (1991) and the glaucophane-lawsonite reaction line is from Evans (1990).
832 The metamorphic conditions are from Caron & Pequignot (1986) for Corsica, and Messiga et
833 al. (1995) for Erro-Tobbio.

834

835 **Figure 3.** Fabric and vein data from Corsica. Coin used for scale is 23.25 mm in diameter. **a**)
836 Foliated blueschist metagabbros (blue-grey) are cut by abundant eclogitic veins (green
837 omphacite, red garnet and pale carbonate). Veins range in size from mm to cm across, and
838 several tens of cm long. **b**) Earlier eclogitic veins have been rotated and sheared into the
839 blueschist fabric. Note the strong mineral lineation in the green eclogitic vein now lying
840 parallel to the blueschist fabric. **c**) Thin section photomicrograph under XPL showing the tip
841 of an eclogitic vein cutting across the blueschist foliation. **d**) Close-up of the area shown in **c**)
842 showing fibrous omphacite growing normal to the sharp vein walls.

843

844 **Figure 4.** Fabric and vein data from Erro-Tobbio. **a**) Foliated antigorite serpentinite (pale
845 brown, grey) cut by fibrous vein of olivine (yellow, green), Ti-clinohumite (dark red) and
846 magnetite (black). Note the vein fibres are perpendicular to the sharp vein edges, and that the
847 foliation in the serpentinite curves into the vein margins, suggesting later localised shear. **b**)
848 Rotated and folded olivine-rich vein with tails merging into a shear band fabric in the host
849 antigorite serpentinite. **c**) Thin section photomicrograph under PPL showing the antigorite
850 foliation cut by the olivine bearing vein. d) Another vein cutting the serpentinite fabric, now
851 viewed under XPL, showing olivine, Ti-clinohumite, magnetite and clinopyroxene.

852

853 **Figure 5.** Orientations of fabrics and veins in the Erro-Tobbio serpentinites. **a-b**) Lower
854 hemisphere, equal-area stereonets showing poles to olivine-clinohumite-magnetite veins
855 (blue triangles) and foliation in the antigorite serpentinite (red dots), and antigorite
856 stretching lineations in the serpentinites (black squares). The mean orientation of the veins is
857 ~45° to the foliation. Measurements taken from two separate outcrops, ~100 m apart, but

each outcrop was contiguous. **c**) Olivine bearing vein cutting the foliation in the serpentinites at an acute angle. **d**) Mineral stretching lineation, defined by elongate aggregates of blue antigorite (parallel to the pen), trends perpendicular to the vein walls and parallel to the vein-filling fibres.

Figure 6. Evidence for a brittle fracture origin of the dehydration veins. All but **f**) from Erro-Tobbio serpentinites. **a**) Olivine, Ti-clinohumite and magnetite all show a fibrous or elongate habit inside the veins, suggesting growth normal to vein margins. **b**) Angular irregularities in sharp vein walls match across the vein and demonstrate positive dilatation. **c**) Vein tips are often curved and split into sharp-edged splays. **d**) Other parallel-sided veins taper at their tips. **e**) Narrow horn-like apophyses are common at vein tips and jogs. **f**) Fibrous eclogitic vein (green) cutting blueschist fabric (blue-grey) and tapering to a narrow tip (Corsica). Note the eclogitic fibres are perpendicular to the vein walls. Coin used for scale in **c** and **d** is 23.25 mm in diameter.

Figure 7. Calculated seismic velocity anisotropy of blueschist. Directional variations of V_p, δV_s and the polarization vectors of S_1 are compared for intact rocks (**a-c**) and dehydration-damaged rocks with fluid-filled crack densities of 0.1 (**d-f**) and 0.5 (**g-i**). Percentages are maximum anisotropies. S_1 polarizations are shown as vectors, where the length marks the orientation with respect to the vertical section. Longer vectors show polarizations in the plane of the page, short vectors (or dots) show polarizations normal to the page. (**a-c**) Maximum V_p in the intact blueschist lies within the plane of the slab and oriented up/ down-dip; maxima of δV_s are also within the slab. For intact rocks with anisotropy solely due to LPOs, S_1 polarization for vertically propagating S waves traversing the slab are predicted to be

trench-normal (sub-horizontal long vectors in the 12 'o' clock positions). (**d-f**) For dehydration-damaged rocks with horizontal fluid-filled cracks at low crack density (cd), maximum V_p is now ~horizontal along the slab. Maximum δV_s for cracked rocks is increased compared to the intact case (80%), and lies oblique to the plane of the slab. For damaged rocks with horizontal fluid-filled cracks, S_1 polarization for sub-vertical S waves are now predicted to be trench-parallel (short vectors just below the 12 'o' clock position). (**g-i**) At higher crack densities (cd = 0.5), the Vp maximum is now degrading towards a crack parallel (horizontal) orientation, although the magnitude remains high. Maximum δV_s is again high, but lies mainly parallel to the cracks. Polarisation of fast shear waves can be trench-parallel for sub-vertical rays.

Figure 8. Calculated seismic velocity anisotropy of serpentinite. Notation and layout same as for Figure 7. (**a-c**) Maximum V_p in the intact serpentinite lies within the plane of the slab and oriented up/ down-dip; maxima of δV_s are also within the slab. For intact rocks with anisotropy solely due to LPOs, S_1 polarization for vertically propagating S waves traversing the slab are predicted to be trench-parallel (short vectors and dots around the 12 'o' clock positions). (**d-f**) For dehydration-damaged rocks with horizontal fluid-filled cracks at low crack density (cd = 0.1), maximum V_p is now ~horizontal along the slab. Maximum δV_s for cracked rocks is increased compared to the intact case (94%), and lies oblique to the plane of the slab. For damaged rocks with horizontal fluid-filled cracks, S_1 polarization for sub-vertical S waves are now predicted to be trench-parallel (short vectors just below the 12 'o' clock position). (**g-i**) At higher crack densities (cd = 0.5), the V_p maximum remains trench-parallel (horizontal) orientation. Maximum δV_s is again high, but has begun to concentrate in the plane of the cracks. Polarisation of fast shear waves can still be trench-parallel for sub-vertical rays.

907 **Figure 9.** Schematic vertical section through a subduction zone. In our model, trench-parallel
908 fast axes will be restricted to the area lying directly above the portion of the slab undergoing
909 dehydration i.e. containing horizontal fluid-filled cracks. As the slab descends, and the
910 hydrous phases are progressively removed, the anisotropy in the slab will be due only to
911 lattice preferred orientations of anhydrous minerals. The absence of any fluid-filled crack
912 damage in the anhydrous rocks at these depths (> 100 km) results in trench-normal fast axes
913 recorded at the surface above.

914

Figure
Click here to download high resolution image

Figure 1, Healy et al., 2008

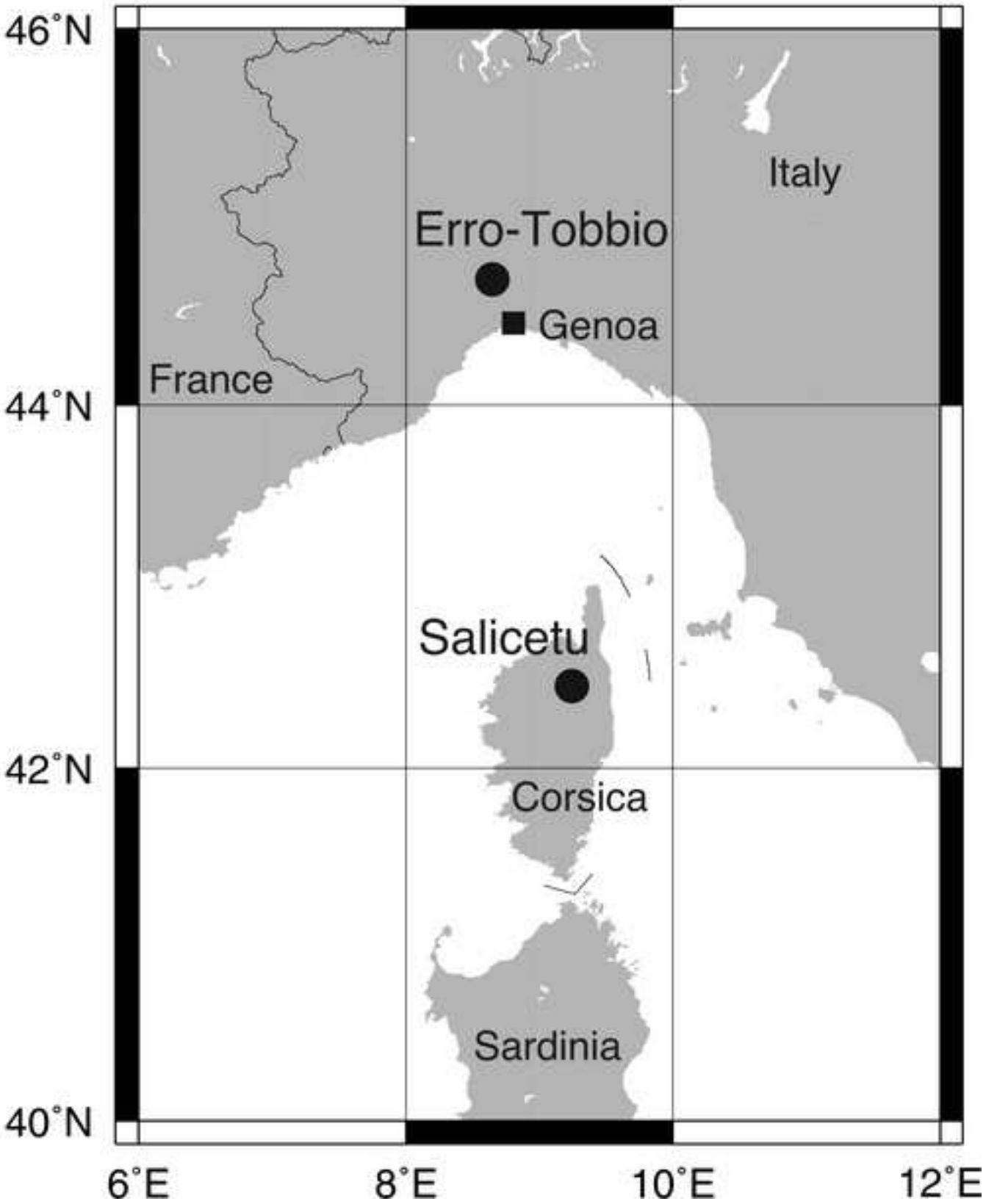

Figure
Click here to download high resolution image

Figure 3, Healy et al., 2008

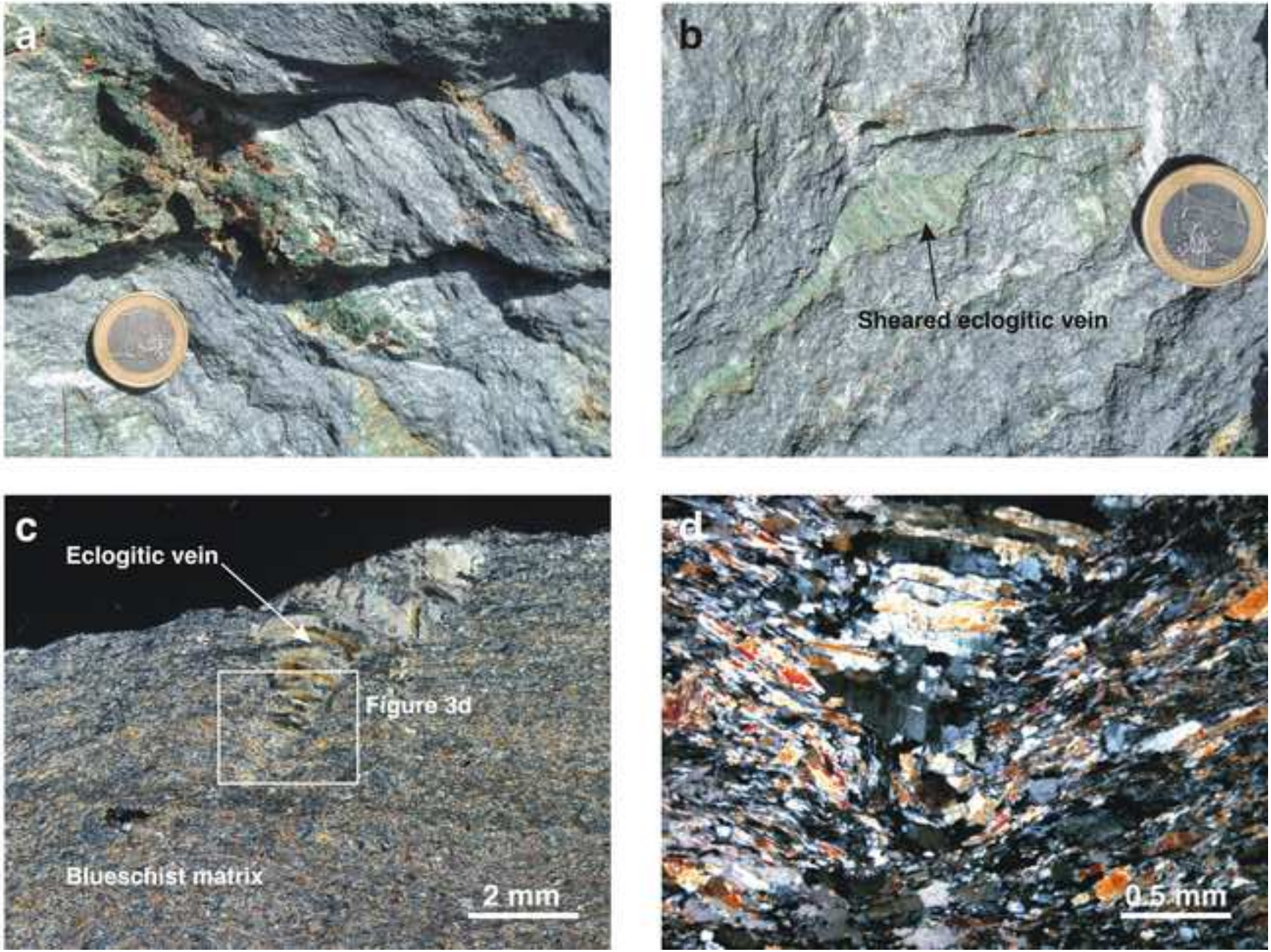

Figure
Click here to download high resolution image

Figure 4, Healy et al., 2008

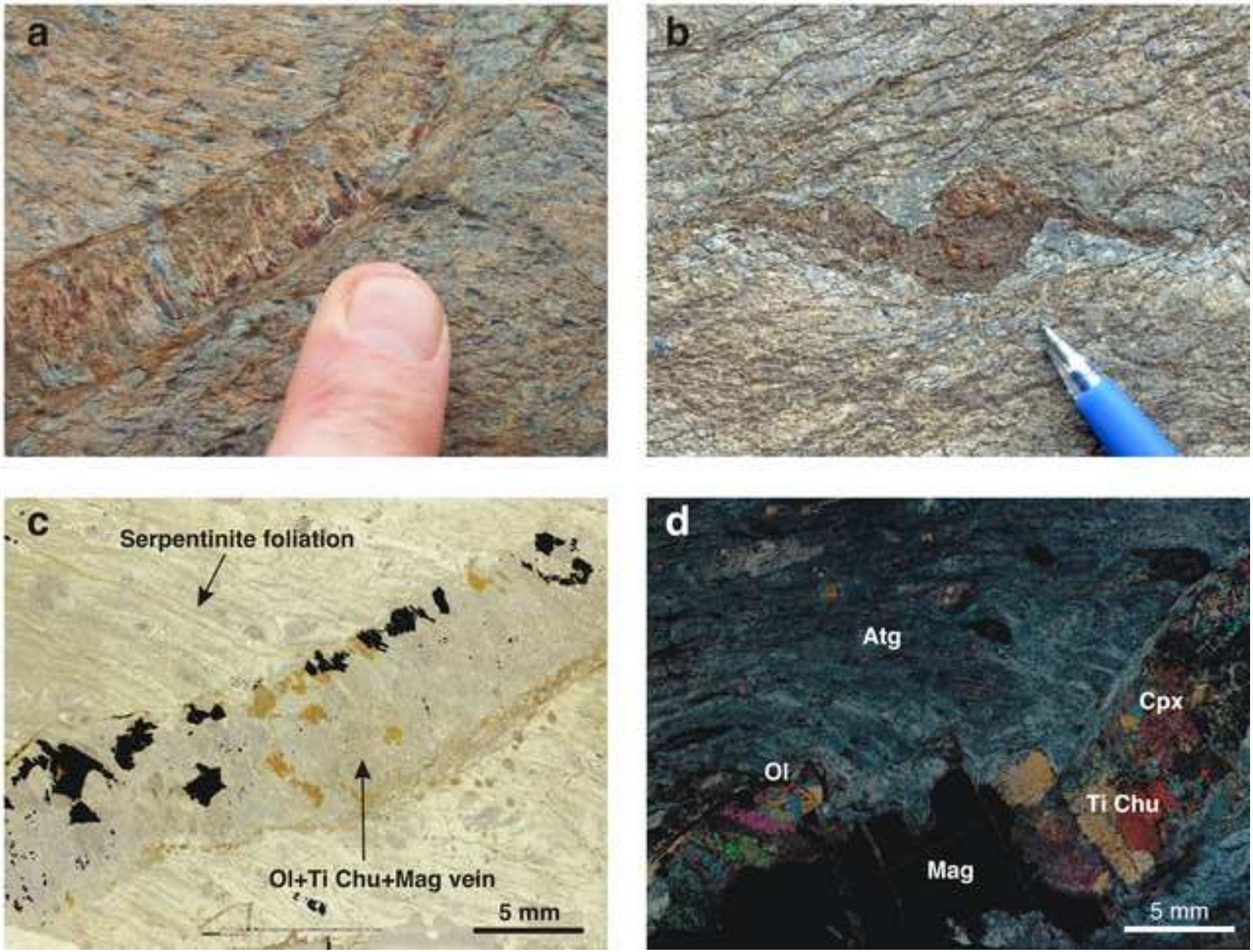

Figure
Click here to download high resolution image

Figure 5, Healy et al., 2008

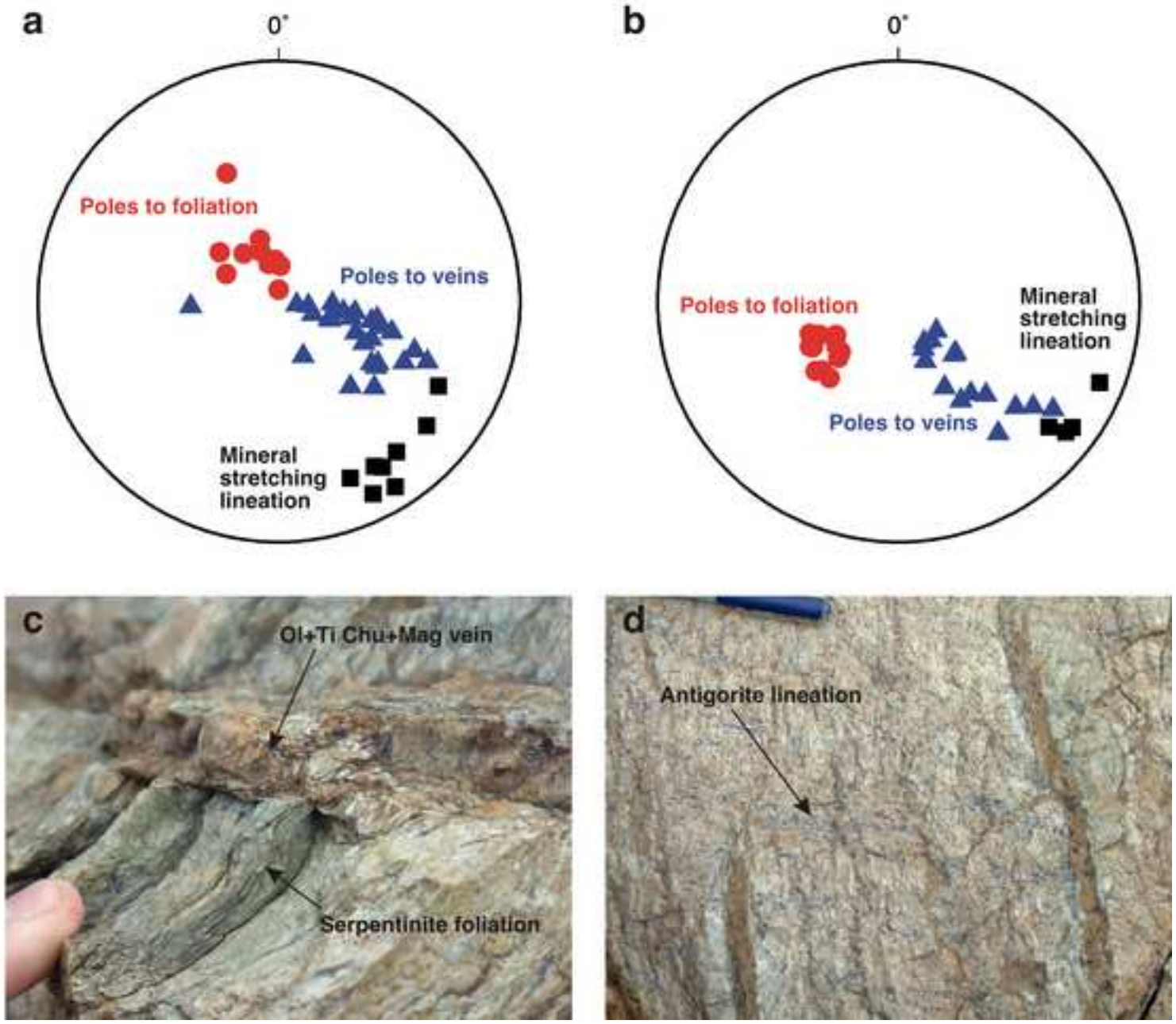

Figure
Click here to download high resolution image

Figure 6, Healy et al., 2008

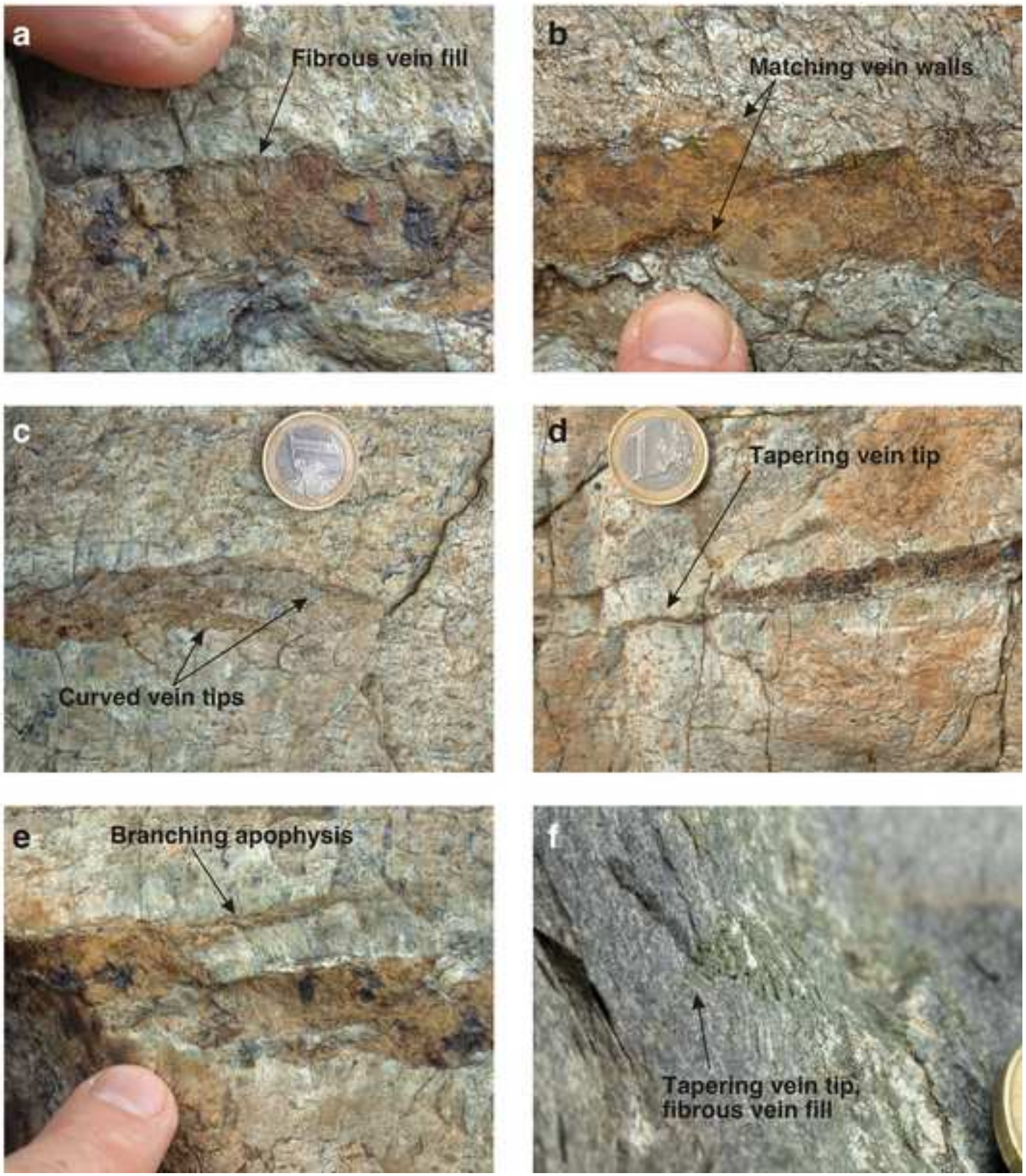

Figure
Click here to download high resolution image

Figure 7, Healy et al., 2008

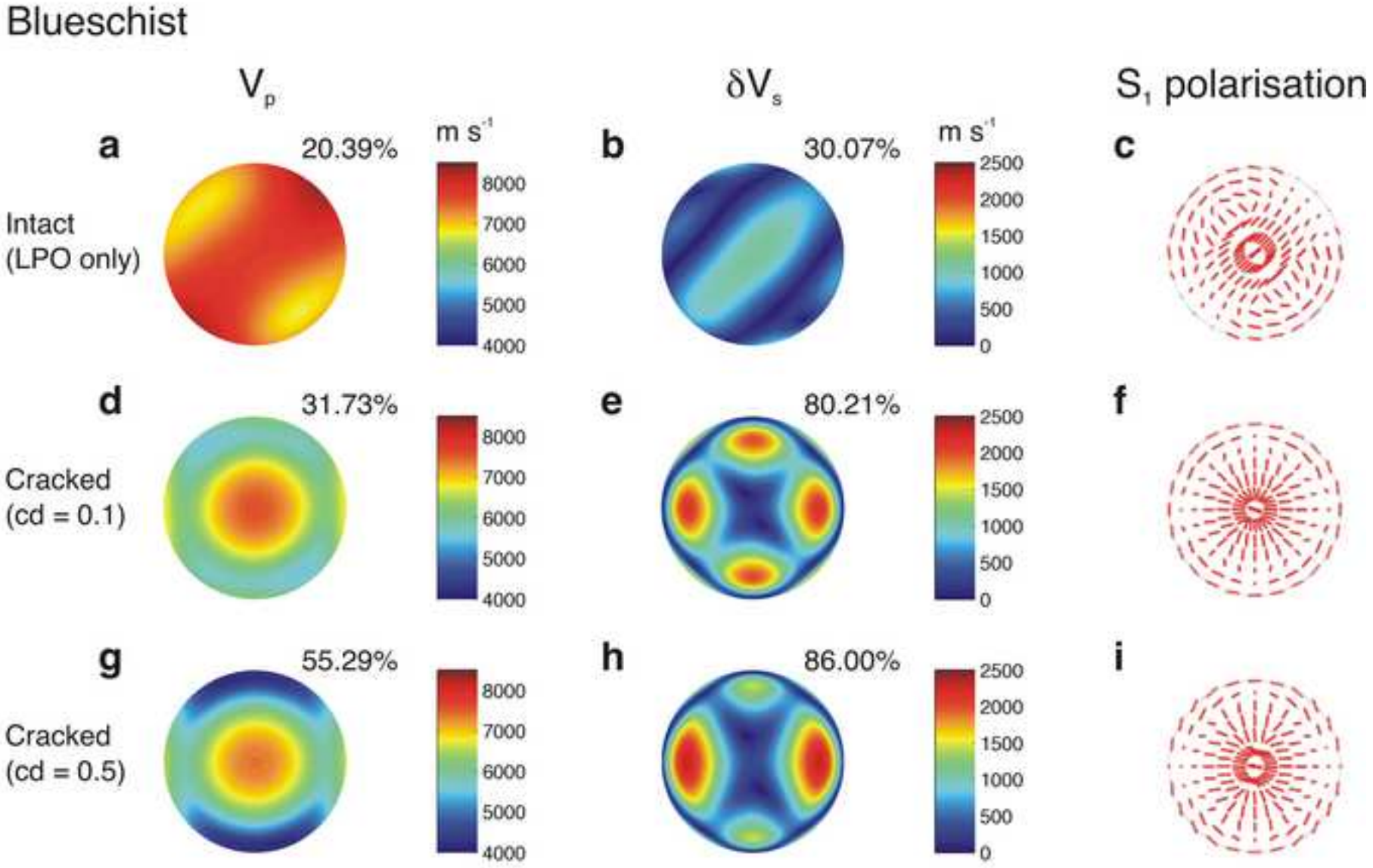

Figure
Click here to download high resolution image

Figure 8, Healy et al., 2008

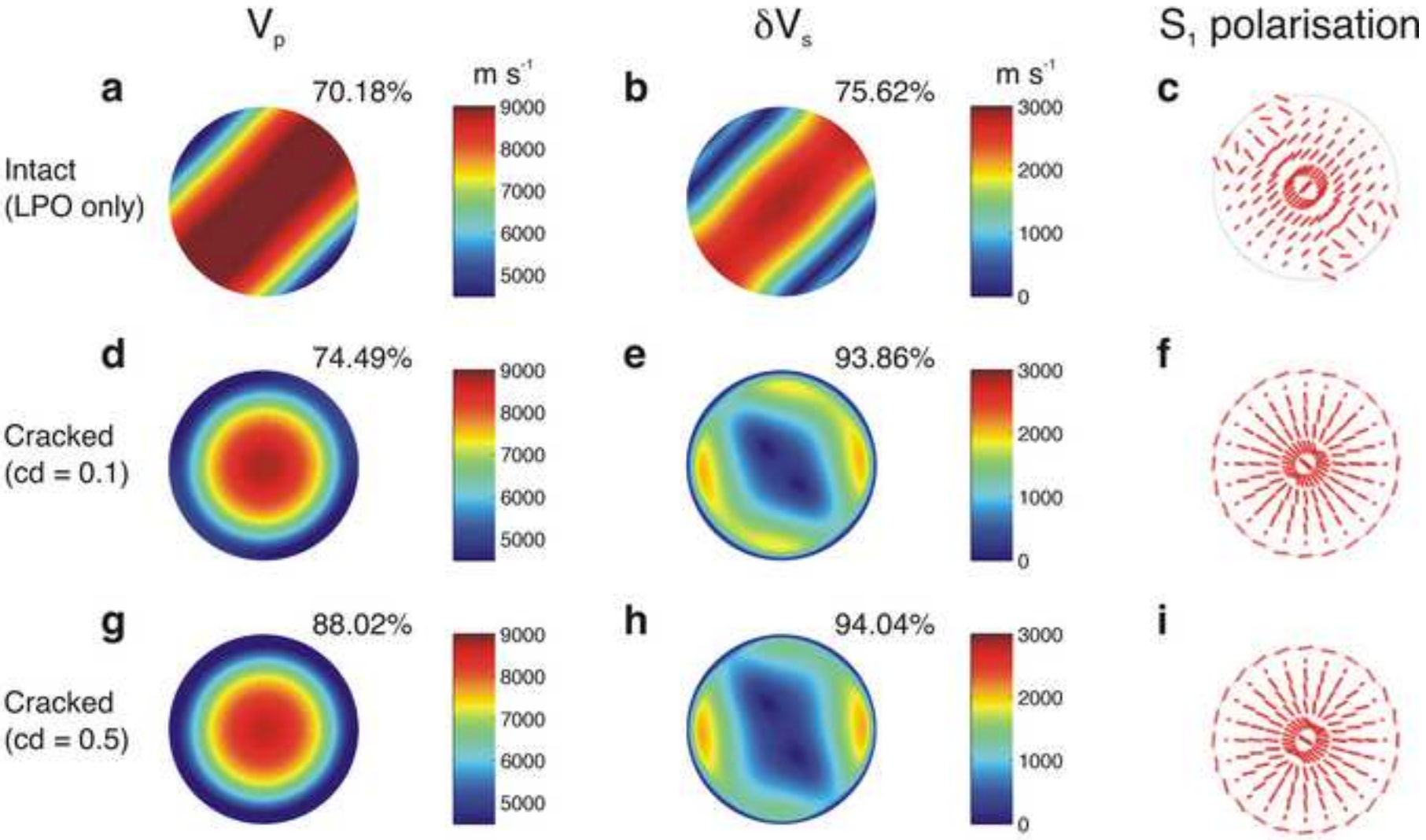

Figure

Click here to download Figure: Figure 9.pdf

Figure 9, Healy et al. 2008

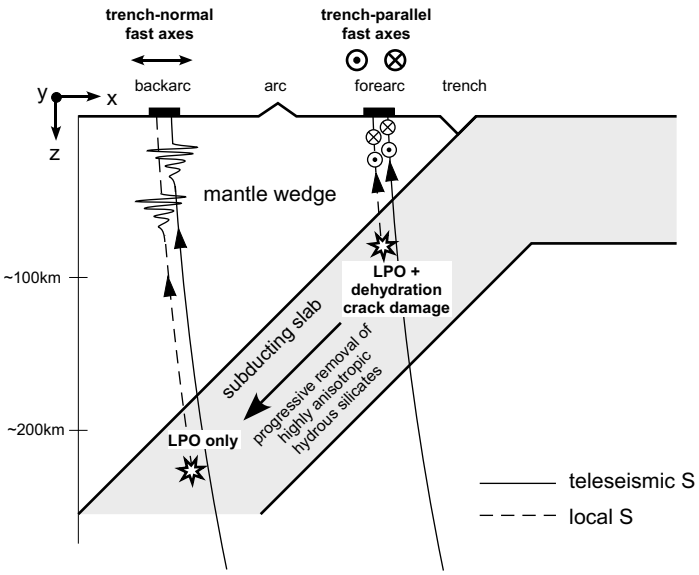

Figure

Click here to download high resolution image

Figure 2, Healy et al., 2008

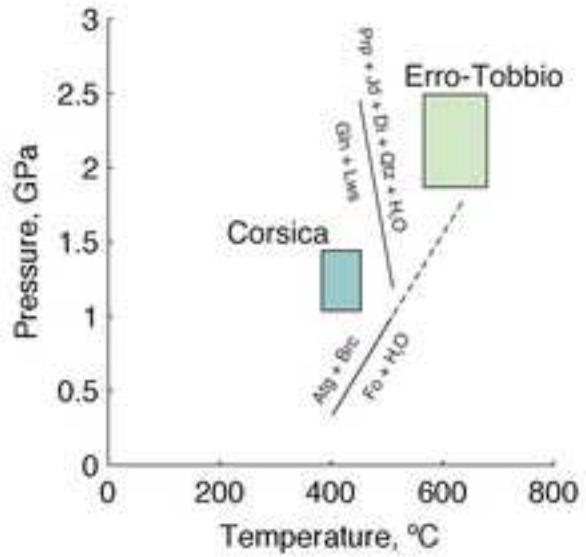

Tables

Table 1. Relationship between mineral crystallographic axes and bulk fabric. XY is the bulk foliation plane parallel to the slab, X is the lineation direction, assumed down-dip and Z is normal to the foliation. References denote the source for the single mineral elastic constants used in seismic anisotropy calculations.

Mineral	X	Y	Z	Ref.
Olivine	[100]	[001]	[010]	Abramson et al., 1997
Orthopyroxene	[001]	[010]	[100]	Jackson et al., 1999
Clinopyroxene	[001]	[100]	[010]	Collins & Brown, 1998
Amphibole	[001]	[010]	[100]	Ahrens, 1995
Antigorite (Lizardite)			[001]	Auzende et al., 2006
Chlorite			[001]	Ahrens, 1995
Muscovite			[001]	Ahrens, 1995
Lawsonite	[001]			Sinogeikin et al., 2000
Epidote	[010]			Mao et al., 2007
Brucite			[0001]	Jiang et al., 2006
Quartz	Random			Ahrens, 1995

Garnet	Random	Chai et al., 1997

8

9